Simulating CO_2 profiles using NIES TM and comparison with HIAPER Pole-to-Pole Observations

Ci Song[1,2], Shamil Maksyutov[3], Dmitry Belikov [3,4,5], Hiroshi Takagi [3], and Jiong Shu[1]

[1]Key Laboratory of Geographic Information Science, Institute of Climate Change, East China Normal University, Shanghai 200241, China

[2]College of Science, Zhongyuan University of Technology, Henan, China

[3]National Institute for Environmental Studies, Tsukuba 305-8506, Japan

[4] National Institute of Polar Research, Tokyo, Japan

[5] Tomsk State University, Tomsk, Russia

Correspondence to: S. Jiong (jshu@geo.ecnu.edu.cn)

Abstract. We present a study on validation of the National Institute for Environmental Studies Transport Model (NIES TM) by comparing to observed vertical profiles of atmospheric CO_2. The model uses a hybrid sigma-isentropic (σ–θ) vertical coordinate that employs both terrain-following and isentropic parts switched smoothly in the stratosphere. The model transport is driven by reanalyzed meteorological fields and designed to simulate seasonal and diurnal cycles, synoptic variations, and spatial distributions of atmospheric chemical constituents in the troposphere. The model simulations were run for combination of biosphere, fossil fuel, air-ocean exchange, biomass burning and inverse correction fluxes of carbon dioxide (CO_2) by GOSAT

Level 4 product. We compared the NIES TM simulated fluxes with data from the HIAPER Pole-to-Pole Observations (HIPPO) Merged 10-second Meteorology, Atmospheric Chemistry, and Aerosol Data, including HIPPO-1, HIPPO-2 and HIPPO-3 from 128.0E to -84.0W, and 87.0N to -67.2S.

The simulation results were compared with CO_2 observations made in January and November, 2009, and March and April, 2010. The analysis attests that the model is good enough to simulate vertical profiles with errors generally within 1–2 ppmv, except for the lower stratosphere in the Northern Hemisphere high latitudes.

1 Introduction

Atmospheric carbon dioxide (CO_2) is the primary radiative forcing greenhouse gas produced by human activities. It causes the most global warming (IPCC, 2013) and its atmospheric concentration has been increasing at a progressively faster rate each decade because of rising global emissions (Raupach et al., 2007). The monitoring of atmospheric CO_2 from space is intended to identify the sources and sinks of the greenhouse gases generated by human and natural activities. A number of satellites are actively monitoring greenhouse gases (e.g., GOSAT, SCIAMACHY, AIRS, IASI) to answer this question, and retrieval algorithms for CO_2 have been developed for these satellite observation data to provide more accurate estimates of CO_2concentrations using several different methods.

The sparseness and spatial inhomogeneity of the existing surface network have limited our ability to understand the quantity and spatiotemporal distribution of CO_2

sources and sinks (Scholes et al., 2009). Recent studies of global sources and sinks of greenhouse gases, and their concentrations and distributions, have been mainly based on in situ surface measurements (GLOBALVIEW-CO_2, 2010). The diurnal and seasonal "rectifier effect", the covariance between surface fluxes and the strength of vertical mixing, and the proximity of local sources and sinks to surface measurement sites all have an influence on the measured and simulated concentrations, and complicate the interpretation of results (Denning et al., 1996; Gurney et al., 2004; Baker et al., 2006). Comparatively speaking, the vertical integration of mixing ratio divided by surface pressure, denoted as the column-averaged dry-air mole fraction (DMF; denoted XG for gas G) is much less sensitive to the vertical redistribution of the tracer within the atmospheric column (e.g., due to variations in planetary boundary layer (PBL) height) and is more easily related to the underpinning surface fluxes than are near-surface concentrations (Yang et al., 2007). Thus, column-averaged measurements and simulations are expected to be very useful for improving our understanding of the carbon cycle (Yang et al., 2007; Keppel-Aleks et al., 2011; Wunch et al., 2011). In addition, atmospheric transport has to be accounted for when analyzing the relationships between observations of atmospheric constituents and their sources/sinks near the earth's surface or through the chemical transformation in the atmosphere. As a result, reliable estimates of climate change depend upon our ability to predict atmospheric CO_2 concentrations, which requires further investigation of the CO_2 sources, sinks, and atmospheric transport.

Global atmospheric tracer transport models are usually applied to studies of the

67 global cycles of the long-lived atmospheric trace gases, such as CO_2 and methane (CH_4),
68 because the long-lived atmospheric tracers exhibit observable global patterns (e.g., the
69 interhemispheric gradient of the concentration). Global three-dimensional chemistry
70 transport models (hereafter referred to as CTMs), driven by actual meteorology from
71 numerical weather predictions, and global circulation models (GCMs) play a crucial
72 role in assessing and predicting change in the composition of the atmosphere due to
73 anthropogenic activities and natural processes (Rasch et al., 1995; Jacob et al., 1997;
74 Denning et al., 1999; Bregman et al., 2006; Law et al., 2008; Maksyutov et al., 2008;
75 Patra et al., 2008).

76 The transport modeling is done on different scales ranging from local plume spread,
77 regional mesoscale transport to global scale analysis, depending on the scale of the
78 phenomena that are studied. Forward modeling is used to estimate tracer concentrations
79 in regions that lack observation data and to identify the features of tracer transport and
80 dispersion (Law et al., 2008; Patra et al., 2008). Inverse methods are generally applied
81 when interpreting the data, with atmospheric transport models providing the link
82 between surface gas fluxes and their subsequent influence on atmospheric
83 concentrations (Rayner and O'Brien, 2001; Patra et al., 2003a,b; Gurney et al., 2004;
84 Baker et al., 2006). Global modeling analysis has helped to identify the relative
85 contribution of the land and oceans in the Northern and Southern hemispheres to the
86 interhemispheric concentration differences in CO_2, CH_4, carbon monoxide (CO) and
87 other tracer species (Bolin and Keeling, 1963; Hein et al., 1997). For stable and slowly
88 reacting chemical species, a number of studies have derived information on the spatial

and temporal distribution of the surface sources and sinks by applying a transport model and atmospheric observations (Tans et al., 1990; Rayner et al., 1999).

There are several factors that strongly influence model performance: the numerical transport algorithm used， meteorological data, grid type and resolution. In tracer transport calculations, semi-Lagrangian transport algorithms are often used in combination with finite-volume models. Losses in the total tracer mass are possible in these algorithms. While such losses are often negligible for short-term transport simulations, they can seriously distort the global trends and tracer budgets in long-term simulations. To avoid such losses, various mass-fixing schemes have been applied (Hack et al., 1993; Rasch et al., 1995). Although the use of mass fixers can prevent mass losses, there remains a possibility of predicting distorted tracer concentrations. By contrast, when using a flux-form transport algorithm, the total tracer mass is conserved and thus the issue of mass losses can be eliminated, provided the flow is conservative. The use of numerical schemes with limiters leads to distorted tracer concentrations and affects the linearity. Thus, to accurately calculate the tracer concentration in a forward simulation and to use the model in inverse modeling, we employed a flux-form version of the global off-line, three-dimensional chemical NIES TM.

The synoptic and seasonal variability in XCO_2 is driven mainly by changes in surface pressure, the tropospheric volume-mixing ratio (VRM) and the stratospheric concentration, which is affected in turn by changes in tropopause height. The effects of variations in tropopause height are more pronounced with increasing contrast between stratospheric concentrations. Many CTMs demonstrate some common failings of model

111 transport in the stratosphere (Hall et al. 1999). The difficulty of accurately representing
112 dynamical processes in the upper troposphere (UT) and lower stratosphere (LS) has
113 been highlighted in recent studies (Mahowald et al., 2002; Wauch and Hall, 2002;
114 Monge-Sanz et al., 2007). While there are many contributing factors, the principal
115 factors affecting model performance in vertical transport are meteorological data and
116 the vertical grid layout (Monge-Sanz et al., 2007).

117 The use of different meteorological fields in driving chemical transport models can
118 lead to diverse distribution of chemical species in the UTLS region (Douglass et al.,
119 1999). The quality of wind data provided by numerical weather predictions is another
120 crucial factor for tracer transport (Jöckel et al., 2001; Stohl et al., 2004; Bregman et al.,
121 2006). Wind fields produced by the Data Assimilation System (DAS) are commonly
122 used for driving CTMs. Spurious variability, or "noise", introduced via the assimilation
123 procedure affects the quality of meteorological data through a lack of suitable
124 observations, or by the inaccurate treatment of model biases (Bregman et al., 2006).
125 This negative effect is proportional to the dynamic time scale and increases with
126 operational time. The most sensitive area in this regard is the lower stratosphere in
127 tropical regions, where large volumes of air move upward from the troposphere to the
128 stratosphere. A lack of observations makes this region the most challenging in terms of
129 data assimilation. Bregman et al. (2006) pointed that additional difficulties for detecting
130 model biases are caused by the fact that tropical atmosphere is not in geostrophic
131 balance. Schoeberl et al. (2003) suggested that GEOS DAS (Geodetic Earth Orbiting
132 Satellite Data Assimilation System) is less suitable for long-term stratospheric transport

studies than wind from a general circulation model. At the same time, improvements to the data assimilation system itself (ECMWF ERA-Interim reanalysis; Dee and Uppala, 2009) and the development of special products for use in transport models (MERRA: Modern Era Retrospective-analysis for Research and Applications; Bosilovich et al., 2008) have assisted in improving the accuracy of atmospheric circulation when using off-line models (Monge-Sanz et al., 2007).

Belikov et al. (2013) evaluated the simulated column-averaged dry air mole fraction of atmospheric carbon dioxide (XCO_2) against daily ground-based high-resolution Fourier Transform Spectrometer (FTS) observations measured at twelve sites of the Total Column Observing Network (TCCON), which provides an essential validation resource for the Orbiting Carbon Observatory (OCO), SCIAMACHY, and GOSAT. In this manuscript, we present the application of the standard version of isentropic transport model with HIAPER Pole-to-Pole Observations (HIPPO) Merged 10-second Meteorology, Atmospheric Chemistry, and Aerosol Data, which are highly time-resolved, because of the underlying 1-second in situ frequency measurement, and vertically-resolved, because of the GV flight plans that performed 787 vertical ascents/descents from the ocean/ice surface up to the tropopause. The remainder of this paper provides the model information and a detailed description of the meteorology dataset and HIPPO data, and a validation of the CO_2 vertical profiles comparing against the HIPPO observations, followed by a discussion and conclusions.

2 Model features and operation

In this section, we describe the features and use of the NIES TM (denoted NIES-08, li). As Belikov et al. (2011, 2013) described, the latest improved version of the NIES TM model uses the (θ–σ) hybrid sigma-isentropic vertical coordinate that is isentropic in the UTLS region but terrain-following in the free troposphere. This designed coordinate helps to simulate vertical motion in the isentropic part of the grid above level 350K. Basic physical model features include the flux-form dynamical core with a third-order van Leer advection scheme, a reduced latitude-longitude grid, a horizontal flux-correction method for mass balance, and turbulence parameterization.

2.1 Meteorological data used in the simulation

The NIES TM is an off-line model driven by Japanese reanalysis data, which covers more than 30 years from 1 January 1979 to present (Onogi et al., 2007). The period of 1979-2004 is covered by the Japanese 25-year Reanalysis (JRA-25), used by Belikov et al. (2013), and is the product of the Japan Meteorological Agency (JMA) and Central Research Institute of Electric Power Industry (CRIEPI). After 2005, near real-time operational analysis, employing the same assimilation system as JRA-25, has been continued as the JMA Climate Data Assimilation System (JCDAS). The JRA-25/JCDAS dataset is distributed on a Gaussian horizontal grid T106 (320 ×160) with 40 hybrid σ–p levels. The 6-hourly time step of JRA-25/JCDAS is coarser than the 3-hourly data from the National Centers for Environmental Prediction (NCEP) Global Forecast System (GFS) and Global Point Value (GPV) datasets, which were used in the previous model version (Belikov et al., 2011). However, with a better vertical resolution

(40 levels on a hybrid σ-p grid versus 25 and 21 pressure levels for GFS and GPV, respectively) it is possible to implement a vertical grid with 32 levels (versus the 25 levels used before), resulting in a more detailed resolution of the boundary layer and UTLS region (Table 1).

The 2-D monthly distribution of the climatological heating rate, used to calculate vertical transport in the θ-coordinate domain of the hybrid sigma-isentropic coordinate, is prepared from JCDAS reanalysis data, which are provided as the sum of short- and long-wave components on pressure levels.

2.2 HIPER Pole-to-Pole data

The HIPPO study investigated the carbon cycle and greenhouse gases at various altitudes (from 0 to 16 km) in the western hemisphere through the annual cycle. HIPPO is supported by the National Science Foundation (NSF) and its operations are managed by the Earth Observing Laboratory (EOL) of the National Center for Atmospheric Research (NCAR). Its base of operations is the EOL Research Aviation Facility (RAF) at the Rocky Mountain Metropolitan Airport (RMMA) in Jefferson Country, Colorado. The main goal of HIPPO was to determine the global distribution of CO_2 and other trace atmospheric gases by sampling at several altitudes and latitudes (from 0 to 16 km, 87.0N to -67.2S) in the Pacific Basin.

The dataset used in this paper includes the merged 10-second data product of meteorological, atmospheric chemistry, and aerosol measurements from three HIPPO Missions 1 to 3. The three missions took place from January, 2009 to April, 2010;

HIPPO-1 (20090109–20090126), HIPPO-2 (20091102–20091122), and HIPPO-3 (20100324–20100415), ranging from 128.0E to -84.0W, and 87.0N to -67.2S (Table 2). All data are provided in a single space-delimited format ASCII file (https://www.eol.ucar.edu/field_projects/hippo).

HIPPO measured atmospheric constituents along transects running approximately pole-to-pole over the Pacific Ocean and recorded hundreds of vertical profiles from the ocean/ice surface up to the tropopause five times during four seasons from January, 2009 to September, 2011. HIPPO provides the first high-resolution vertically resolved global survey of a comprehensive suite of atmospheric trace gases and aerosols pertinent to understanding the carbon cycle and challenging global climate models. The 10-second merge product applied in this study was derived by combining the National Science foundation (NSF)/NCAR GV aircraft navigation and atmospheric structure parameters including position, time, temperature, pressure, and wind speed reported at 1-second frequency, with meteorological, atmospheric chemistry and aerosol measurements made by several teams of investigators on a common time and position basis.

2.3 Model setup

The standard model was run with the three HIPPO missions to study atmospheric tracer transport and the ability of the model to reproduce the column-averaged dry air mole

fractions and vertical profile of atmospheric CO_2. The model was run at a horizontal resolution of 2.5 °×2.5 °and 32 vertical levels from the surface to 3 hPa.

The CO_2 simulations were began on January 1, 2009, November 1, 2009 and March 1, 2010 for the three HIPPO missions 1 to 3, respectively, with individual initial 3D tracer distributions using the global prior fluxes of biosphere-atmosphere and air-ocean exchange, fossil fuel emissions, biomass burning, and GOSAT Level 4A inverse model correction (Maksyutov et al., 2013), provided by climatological mean of monthly global CO_2 fluxes estimated with GLOBALVIEW and GOSAT SWIR Level 2 XCO_2 data. As we use same set of fluxes and same version of transport model as GOSAT Level 4 product, the flux corrections provided by GOSAT Level 4 product provide optimal fit to available observations.

3 Discussions

The current model versions have been used in several tracer transport studies and were evaluated through participation in transport model intercomparisons (Niwa et al., 2011; Patra et al., 2011). The simulation results of the tracer transport model show consistency with observations in the near-surface layer and in the free troposphere. However, the model performance in the UTLS region has not been evaluated in detail against other observations.

3.1 Comparison with CO_2 observations

Figure 1 show the scatters diagram of modeled results versus total column of HIPPO-1, 2, 3. The majority of points are within a 95% confidence interval of total CO_2 column

concentration. Modeled HIPPO-1's precision successively exceeds 2 and 3, inferring the simulation results with the relevant either seasonal changes or data quality.

The simulation results of CO_2 concentration time-varying for HIPPO-1 using the standard model display good performance and weak dispersion of concentrations. The validation results (Figure 2(a)) show that approximately 69.2% of the absolute biases are within 1 ppmv, approximately 92.3% are within 2 ppmv, and only 7.7% exceed 3 ppmv. Furthermore, as shown by the root-mean-square error (RMSE) with time, during most days in January the model values' dispersion was small compared with the observed values, apart from the first few days of the month. According to the simulation results of the HIPPO-1 observed and simulated latitude-varying CO_2 concentration data, the comparison values always underestimate the atmospheric XCO_2, and the differences are all within 1.5 ppmv in the Southern Hemisphere, and vice versa in the Northern Hemisphere with 85.8% of the differences under 1.1 ppmv. Figure 2(b) shows that the larger biases usually occur in the Northern Hemisphere high latitudes. The RMSE also reflects the instability of the simulated values in the Northern Hemisphere high latitudes.

For HIPPO-2 data from November 2 to 22, 2009,the absolute biases of observed and simulated time-varying are all within 2 ppmv, and 77.8 % of the differences are less than 1 ppmv (Figure 2(c)).Approximately 5/6 of the data over the month show comparative stability. Similarly with HIPPO-1, the simulation results are always underestimates in the Southern Hemisphere and overestimates in the Northern Hemisphere. As shown in Figure 2(d), the complete simulation displays good

265 performance, apart from one day in the Northern Hemisphere high latitudes. In the same
266 manner, the RMSE shows good stability in the Southern Hemisphere, in particular for
267 the low-to mid-latitudes of the Southern Hemisphere. The model also simulates well in
268 the Northern Hemisphere, especially from 45 °to 70 °N.

269 Based on HIPPO-3 data from March 24 to April 15, 2010, the model simulation
270 overestimates in March and underestimates in April. As shown in Figure 2(e), in March,
271 the biases over several days were over 2 ppmv, and one of these days exceeded 3 ppmv.
272 However, the absolute biases were all within 2 ppmv in April, and 75% of the absolute
273 biases were less than 1 ppmv, which suggests relatively good performance by the model
274 simulation. As shown by the RMSE, the data for the last days in March were disperse.
275 However, 81.8% of the data in April showed comparatively good stability. The absolute
276 biases are all under 1.5 ppmv in the Southern Hemisphere, and are also within 2 ppmv
277 for the low- and mid-latitudes of the Northern Hemisphere (Figure 2(f)).However, a
278 relatively large difference occurs at the Northern Hemisphere high latitudes, at one
279 point exceeding 3 ppmv. Furthermore, the RMSE become greater with latitude from
280 the Southern to Northern hemisphere, inferring the simulation results are increasingly
281 disperse with increasing latitude.

282 **3.2 Validation of CO_2 vertical profiles**

283 The GV flight plan performed 787 vertical ascents/descents from the ocean/ice
284 surface/land surface to the tropopause. Two maximum altitude ascents were planned
285 per flight to the tropopause/LS; one in the first half and the other in the second half of
286 the research flight. In between, several vertical profiles from below the PBL to the mid-

troposphere (1000–28000 feet) were flown. Profiles were flown approximately every 2.2 ºof latitude with 4.4 ºbetween consecutive near-surface or high-altitude samples. Rate of climb and descent was 1500 ft/minute (457m/minute). During these profiles, the GV averaged a ground speed of approximately 175m/second, or 10 km/minute.

Most of a flight was conducted below the international Reduced Vertical Separation Minimum (RVSM), usually 29000 ft or 8850 m, to allow the GV to descend and climb constantly to collect data at different altitudes throughout the troposphere. All flight plans were subject to modifications depending on local atmospheric conditions and approval by air traffic control. Most profiles extended from approximately 300 to 8500 m altitude, constrained by air traffic, but significant profiling extended above approximately 14 km.

One of the aims of this paper was to validate the model column-averaged concentration against the typical HIPPO flight plans, and we therefore examined the variability of CO_2 concentrations with HIPPO merged 10-second meteorology, atmospheric chemistry, and aerosol measurements from Mission 1 to 3. For each mission, several hundred vertical profiles were produced. We have only selected the vertical profiles from near-surface to LS to compare the simulations using the standard model with observations. Each mission can be divided into six parts for analysis; the low-, mid- and high-latitudes in the Southern and Northern hemispheres, respectively.

The above Figure 3 presents us the change of flight altitude and bias by subtracting observation by simulation of HIPPO-1, 2, 3 with latitude. The observations' number of these three missions is 17621, 23451, 22372 respectively, and the plenty of observations provide basis for model validation. Based on the change of flight height with latitude

in the Figure 3, we only select CO_2 profiles that their height is from near surface to lower stratosphere. According to the above rule, 24, 34, 35 profiles are chosen respectively for the HIPPO-1, 2, 3. Then we separately choose one profile in the low, middle and high latitude of Northern and Southern hemisphere from the selected profiles for each mission because of the similarity of the profile shape in every latitude zone. Seen from the Figure 3, the relatively larger biases repeatedly occur in the higher latitude of Northern hemisphere.

For HIPPO-1, the modeled value is always less than the observation value in the Southern Hemisphere and vice versa in the Northern Hemisphere. The bias is less than 2 ppmv for the entire profile from the near-surface to the LS; however, it increases from 2 to 4 ppmv above 10 km covering the Northern Hemisphere high latitudes.

Figure 4 shows the comparison of simulation results and observations for data from the near-surface to the LS in the low-, mid- and high- latitude. In the low-latitudes, as shown by panel 4(c) and (d), the simulation performed very well compared with observations. With the exception of the biases of approximately 2 ppmv in the tropopause in panel 4(d), the biases are all within 1 ppmv. In the mid- and high- latitudes, it is different in both hemispheres. In the Southern Hemisphere, the majority biases are within 2 ppmv apart from the LS zone in Figure 4(a) and 2 to 6 km region in panel 4(b). In the Northern Hemisphere (panel 4(e) and (f)), the simulated vertical profiles show good performances, apart from UTLS, and the biases are less than 2 ppmv. Some large biases occurred in the UTLS exceeding 4 ppmv when the potential temperature gradient increased rapidly with height. For details, Figure 5 presents us the biases of simulation minus observation corresponding to Figure 4(a) – 4(f) respectively.

HIPPO-2 data showed overall similarity with HIPPO-1 data based on the distribution of positive and negative bias. However, an anomaly occurred at approximately -60 °and 75 ° latitude, showing positive and negative biases, respectively, some exceeding 6 ppmv. Figure 6(a) is the vertical profile of the Southern Hemisphere high latitudes, which clearly shows that the simulation matches well with the observations from the near-surface to the tropopause. However, large biases occur above 8 km; panel 6(b) also shows this phenomenon above 10 km. In the low latitudes (Figure 6(c) and (d)), the simulations match well with observations. The potential temperature gradient is smooth and the biases are less than 1 ppmv from near-surface to the UT, which indicates good performance. For the mid-latitudes of the Northern Hemisphere, panel 6(e) shows relatively good simulation performance. However, as shown in panel 6(f), the high latitudes did not perform well in the near-surface or the low- and mid-troposphere. Compared with observations, the simulation profiles do not appear to reflect the original shape. Moreover, Figure 7 further displays the biases of simulation minus observation corresponding to Figure 6(a) – 6(f) respectively.

As shown by HIPPO-3 data the biases increase abruptly with flight height for the mid- to high-latitudes of the Northern Hemisphere with values reaching 7 ppmv. In the high-latitudes of the Southern Hemisphere (panel 8(a)) the simulation underestimates the observations, and the absolute biases are isostatic from the near-surface to the LS, which are less than 3 ppmv. The Southern Hemisphere low latitudes (panel 8(c)) indicate good performance of the simulations, where all the biases are less than 1 ppmv. In the Northern Hemisphere low latitudes (panel 8(d)), the entire simulation appears to

355 match well with observations. However, some locations do not reproduce the precise
356 shape through the entire height. For the mid- to high- northern latitudes (panel 8(e) and
357 (f)), the simulations performed relatively well from the near-surface to the UT.
358 Furthermore, Figure 9 shows the biases of simulation minus observation corresponding
359 to Figure 8(a) – 8(f) respectively.

360 Larger bias in simulations is found in the winter lower stratosphere in the northern
361 high-latitudes. The problem appears because between tropopause and 350 K level
362 model uses vertical wind provided by reanalysis instead of using radiative heating rate,
363 which is more accurate in stratosphere (Weaver et al, 1993, Belikov et al., 2013).
364 Extending the isentropic coordinates to mid-troposphere levels such as implemented by
365 Chen and Rasch, (2011), Bleck et al (2015) has potential for reducing the transport bias
366 in this region and season. The positive bias can reach level of 4 ppm for CO_2. However,
367 this problem only affects simulations for observation made in lower stratosphere in high
368 latitudes in cold season when the tropopause level is low. However the number of in-
369 situ observations made in this altitude is very limited. The satellite observations of the
370 total column such as GOSAT are also reduced considerably in high latitudes in cold
371 season (Yoshida et al, 2013). Thus this lower stratosphere bias is not likely to deteriorate
372 the transport model performance in the inverse modeling applications (Maksyutov et
373 al., 2013). However, these biased values probably result in greater errors of a flux
374 inversion with signals being transported into lower latitudes in adverse synoptic
375 patterns.
376

4 Conclusions

This study tested and verified the ability of a chemistry transport model to reproduce CO_2 vertical profiles using HIPPO merged 10-second meteorology, atmospheric chemistry, and aerosol data from Missions 1 to 3, which span three different seasons (autumn, winter and spring). The results show that the model somewhat underestimates CO_2 in the Southern Hemisphere and overestimates it in the Northern Hemisphere for these three missions. However, the model was able to reproduce the seasonal and inter-annual variability of CO_2 with RMS bias across all profiles with a level of 0.9 ppmv. The model performed well from the near-surface layer to the top of the troposphere, apart from the lower stratosphere the high latitude regions, in particular, in the Northern Hemisphere in spring, where large biases would often appear. The smaller bias for HIPPO-1 compared with HIPPO-3 arises from seasonal changes in synoptic patterns from January to March and April, as simulated by Patra et al. (2008).

The accuracy of these calculations will increase with the adaptation of the mass-balanced reanalysis data (MERRA, Bosilovich et al., 2008). This off-line model with horizontal flux-correction attain mass conservation because vertically integrated mass change is in balance with the surface pressure tendency (Belikov et al., 2011). The computation achieve fast convergence with CO_2 distribution tending towards stability in the whole integral height. Demand for global high-resolution fields of CO_2 and other greenhouse gases will also increase because of their use as a priori information in retrieval algorithms of observation instruments, such as the AIRS satellite (e.g., Strow and Hannon, 2008) and GOSAT (e.g., Yokota et al., 2009), and regional inverse

399 modeling studies (Thompson, et al., 2014). Employing HIPPO-1, 2, 3, validation of the
400 NIES model provide basis for applying high-precision satellite product, and so we can
401 get more and better carbon sources/sinks information.
402
403 **Acknowledgements** The authors acknowledge NSF, EOL of NCAR and NOAA which
404 supported the collection of the original HIPPO data. This project was supported by the
405 National Basic Research Program of China (No. 2010CB951603). The computation
406 was supported by the High Performance Computer Center of East China Normal
407 University. We thank the team members of the Biogeochemical Cycle Modeling and
408 Analysis Section of National Institute for Environment Studies, Tsukuba, Japan for
409 providing expert advice and assistance. The GOSAT Level 4 data made available by
410 GOSAT project (http://www.gosat.nies.go.jp/index_e.html).
411
412
413
414
415
416
417
418
419
420

References

1. Baker, D. F., Law, R. M., Gurney, K. R., Rayner, P., Peylin, P., Denning, A. S., Bousquet, P., Bruhwiler, L., Chen, Y.-H., Ciais, P., Fung, I. Y., Heimann, M., John, J., Maki, T., Maksyutov, S., Masarie, K., Prather, M., Pak, B., Taguchi, S., and Zhu, Z.: TransCom 3 inversion intercomparison: Impact of transport model errors on the interannual variability of regionalCO_2 fluxes 1988–2003, Global Biogeochem. Cy., 20, GB1002, doi:10.1029/2004GB002439, 2006.
2. Belikov, D. A., Maksyutov, S., Miyasaka, T., Saeki, T., Zhuravlev, R., and Kiryushov, B., Mass-conserving tracer transport modeling on a reduced latitude-longitude grid with NIES-TM, Geosci. Model Dev., 4, 207-222, doi: 10.5194/gmd-4-207-2011, 2011.
3. Belikov, D. A., Maksyutov, S., Sherlock, V., Aoki, S., Deutscher, N. M., Dobe, S., Griffith, D., Kyro, E., Morino, I., Nakazawa, T., Notholt, J., Rettinger, M., Schneider, M., Sussmann, R., Toon. G. C., Wennberg, P. O., and Wunch, D., Simulations of column-averaged CO_2 and CH_4 using the NIES TM with a hybrid sigma-isentropic ($\sigma - \theta$) vertical coordinate, Atmos. Chem. Phys., 13, 1713-1732, doi: 10.519/acp-13-1713-2013, 2013.
4. 15,
5. Bolin, B., and Keeling, C. D., Large scale atmospheric mixing as deduced from seasonal and meridional variations of the atmospheric carbon dioxide, J. Geophys. Res., vol.68, pp.3899-3920, 1963.
6. Bosilovich, M. G., Chen, J., Robertson F. R., and Adler R. F.: Evaluation of global

precipitation in reanalysis. J. Appl. Meteor. Climatol., 47, 2279–2299, doi:10.1175/2008JAMC1921.1, 2008.

7. Bregman, B., Meijer, E., and Scheele, R.: Key aspects of stratospheric tracer modeling using assimilated winds, Atmos. Chem. Phys., 6, 4529–4543, doi: 10.5194/acp-6-4529-2006, 2006.

8. Chen, C.-C. and Rasch, P. J., Climate Simulations with an Isentropic Finite-Volume Dynamical Core. J. Climate, 25, 2843–2861.doi: http://dx.doi.org/10.1175/2011JCLI4184.1, 2012.

9. Dee, D. P. and Uppala, S.,Variational bias correction of satelliteradiance data in the ERA-Interim reanalysis, Q. J. Roy. Meteorol. Soc., 135, 1830–1841, 2009.

10. Denning, A. S., Randall, D. A., Collatz, G. J., and Sellers, P. J.: Simulations of terrestrial carbon metabolism and atmosphericCO2 in a general circulation model. II. Simulated CO_2 concentrations, Tellus B Chem. Phys. Meteorol., 48, 543–567, doi:10.1034/j.1600-0889.1996.t01-1-00010.x, 1996.

11. Denning, A. S., Holzer, M., Gurney, K. R., Heimann, M., Law, R. M., Rayner, P. J., Fung, I. Y., Fan, S.-M., Taguchi, S., Friedlingstein, P., Balkanski, Y., Taylor, J., Maiss, M., and Levin, I.: Three-dimensional transport and concentration of SF6: A model intercomparison study (TransCom2), Tellus, 51B, 266–297, 1999.

12. Douglass, A. R., Prather, M. J., Hall, T. M., Strahan, S. E., Rasch, P. J., Sparling, L. C., Coy, L., and Rodriguez J. M.: Choosing meteorological input for the global modeling initiative assessment of high-speed aircraft, J. Geophys. Res., 104, 27545–27564, 1999.

13. GLOBALVIEW-CO_2: Cooperative Atmospheric Data Integration Project–Carbon Dioxide, CD-ROM, NOAA ESRL, Boulder, Colorado, 2010.

14. Gurney, K. R., Law, R. M., Denning, A. S., Rayner, P. J., Pak, B. C., Baker, D., Bousquet, P., Bruhwiler, L., Chen, Y. H., Ciais, P., Fung, I. Y., Heimann, M., John, J., Maki, T., Maksyutov, S., Peylin, P., Prather, M., and Taguchi, S.: Transcom 3 inversion intercomparison: Model mean results for the estimation of seasonal carbon sources and sinks, Global Biogeochem. Cy., 18, GB1010, doi:10.1029/2003GB002111, 2004.

15. Hack, J. J., Boville, B. A., Briegleb, B. P., Kiehl, J. T., Rasch, P. J., and Williamson, D. L.: Description of the NCAR community climate model (CCM2), NCAR/TN-382, 108, Climate and Global Dynamics Division, NCAR, Boulder, Colorado, USA, 1993.

16. Hall, T. M., Waugh, D.W., Boering, K. A., and Plumb R. A.: Evaluation of transport in stratospheric models, J. Geophys. Res., 104, 18815–18839, 1999.

17. Hein, R., Crutzen, P. J., and Heimann, M., An inverse modeling approach to investigate the global atmospheric methane cycle, Global Biogeochem Cycles, vol, 11, pp.43-76, 1997.

18. Ciais, P., Sabine C., Bala G., Bopp L., Brovkin V., Canadell J., Chhabra A., DeFries R., Galloway J., Heimann M., Jones C., Le Qu éré C., Myneni R. B., Piao S. and Thornton P., 2013: Carbon and Other Biogeochemical Cycles. In: Climate Change 2013: The Physical Science Basis. Contribution of Working Group I to the Fifth Assessment Report of the Intergovernmental Panel on Climate Change [Stocker,

487 T.F., D. Qin, G.-K. Plattner, M. Tignor, S.K. Allen, J. Boschung, A. Nauels, Y. Xia,
488 V. Bex and P.M. Midgley (eds.)]. Cambridge University Press, Cambridge, United
489 Kingdom and New York, NY, USA.
490 19. Jacob, D., Prather, M. J., Rasch, P. J., Shea, R.-L., Balkanski, Y. J., Beagley, S. R.,
491 Bergmann, D. J., Blackshear, W. T., Brown, M., Chiba, M., Chipperfield, M. P., de
492 Grandpr ́e, J., Dignon, J. E., Feichter, J., Genthon, C., Grose, W. L., Kasibhatla, P.
493 S., K ̈ohler, I., Kritz, M. A., Law, K., Penner, J. E., Ramonet, M., Reeves, C. E.,
494 Rotman, D. A., Stockwell, D. Z., Van Velthoven, P. F. J., Verver, G., Wild, O., Yang,
495 H., and Zimmermann, P.: Evaluation and intercomparison of global transport
496 models using 222Rn and other short-lived tracers, J. Geophys. Res., 102(D5),
497 5953–5970, 1997.
498 20. J ̈ockel, P., von Kuhlmann, R., Lawrence, M. G., Steil, B., Brenninkmeijer, C. A.
499 M., Crutzen, P. J., Rasch, P. J., and Eaton, B.: On a fundamental problem in
500 implementing flux-form advection schemes for tracer transport in 3-dimensional
501 general circulation and chemistry transport models, Q. J. Roy. Meteorol. Soc., 127,
502 1035–1052, 2001.
503 21. Keppel-Aleks, G., Wennberg, P. O., and Schneider, T.: Sources of variations in total
504 column carbon dioxide, Atmos. Chem. Phys., 11, 3581–3593, doi: 10.5194/acp-11-
505 3581-2011, 2011.
506 22. Law, R. M., Peters, W., R ̈odenbeck, C., Aulagnier, C., Baker, I., Bergmann, D. J.,
507 Bousquet, P., Brandt, J., Bruhwiler, L., Cameron-Smith, P. J., Christensen, J. H.,
508 Delage, F., Denning, A. S., Fan, S.-M., Geels, C., Houweling, S., Imasu, R.,

509 Karstens, U., Kawa, S. R., Kleist, J., Krol, M., Lin, S.-J., Lokupitiya, R., Maki, T.,
510 Maksyutov, S., Niwa, Y., Onishi, R., Parazoo, N., Patra, P. K., Pieterse, G., Rivier,
511 L., Satoh, M., Serrar, S., Taguchi, S., Takigawa, M., Vautard, R., Vermeulen, A. T.,
512 and Zhu, Z.: Trans Commodel simulations of hourly atmospheric CO2:
513 Experimental overview and diurnal cycle results for 2002, Global Biogeochem. Cy.,
514 22, GB3009, doi:10.1029/2007GB003050, 2008.
515 23. Mahowald, N. M., Plumb, R. A., Rasch, P. J., del Corral, J., and Sassi, F.:
516 Stratospheric transport in a three-dimensional isentropic coordinate model, J.
517 Geophys. Res., 107, 4254, doi:10.1029/2001JD001313, 2002.
518 24. Maksyutov, S., Patra, P. K., Onishi, R., Saeki, T., and Nakazawa, T., NIES/FRCGC
519 global atmospheric tracer transport model: description, validation, and surface
520 sources and sinks inversion, Journal of the Earth Simulator, 9, 3-18, 2008.
521 25. Maksyutov, S., Takagi, H., Valsala, V. K., Saito, M., Oda, T., Saeki, T., Belikov, D.
522 A., Saito, R., Ito, A., Yoshida, Y., Morino, L., Uchino, O., Andres, R. J., and Yokota,
523 T., Regional CO_2 flux estimates for 2009-2010 based on GOSAT and ground-based
524 CO_2 observations, Atmos. Chem. Phys., 13, 93519373, doi: 10.5194/acp-13-9351-
525 2013, 2013.
526 26. Monge-Sanz, B. M., Chipperfield, M. P., Simmons, A. J., and Uppala, S. M., Mean
527 age of air and transport in a CTM: Comparison of different ECMWF analyses,
528 Geophys. Res. Lett., 34, L04801, doi: 10.1029/2006GL028515, 2007.
529 27. Niwa, Y., Patra, P. K., Sawa, Y., Machida, T., Matsueda, H., Belikov, D., Maki, T.,
530 Ikegami, M., Imasu, R., Maksyutov, S., Oda, T., Satoh, M., and Takigawa, M.:

531 Three-dimensional variations of atmospheric CO_2: aircraft measurements and
532 multi transport model simulations, Atmos. Chem. Phys., 11, 13359–13375,
533 doi:10.5194/acp-11-13359-2011, 2011.
534 28. Onogi, K., Tsutsui, J., Koide, H., Sakamoto, M., Kobayashi, S., Hatsushika, H.,
535 Matsumoto, T., Yamazaki, N., Kamahori, H., Takahashi, K., Kadokura, S., Wada,
536 K., Kato, K., Oyama, R., Ose, T., Mannoji, N., and Taira, R.: The JRA-25
537 Reanalysis, J. Met. Soc. Jap., 85, 369–432, 2007.
538 29. Parker, R., Boesch, H., Cogan, A., Fraser, A., Feng, L., Palmer, P.I., Messerschmidt,
539 J., Deutscher, N., Griffith, D. W. T., Notholt, J., Wennberg, P.O., and Wunch, D.:
540 Methane observations from the Greenhouse Gases Observing SATellite:
541 Comparison to ground based TCCON data and model calculations, Geophys. Res.
542 Lett., 38, L15807, doi: 10.1029/2011GL047871, 2011.
543 30. Patra, P. K., Baker, D., Bousquet, P., Bruhwiler, L., Chen, Y.-H., Ciais, P., Denning,
544 S. A., Fan, S., Fung, I. Y., Gloor, M., Gurney, K., Heimann, M., Higuchi, K., John,
545 J., Maki, T., Maksyutov, S., Peylin, P., Prather, M., Pak, B., Sarmiento, J., Taguchi,
546 S., Takahashi, T., and Yuen, C.-W.: Sensitivity of optimal extension of observation
547 networks to the model transport, Tellus, 55B, 498–511, 2003a.
548 31. Patra, P. K., Maksyutov, S., Sasano, Y., Nakajima, H., Inoue, G., and Nakazawa, T.:
549 An evaluation of CO_2 observations with Solar Occultation FTS for Inclined-Orbit
550 Satellite sensor for surface source inversion, J. Geophys. Res., 108(D24), 4759,
551 doi:10.1029/2003JD003661, 2003b.
552 32. Patra, P. K., Peters, W., R ̈odenbeck, C., Aulagnier, C., Baker, I., Bergmann, D. J.,

553 Bousquet, P., Brandt, J., Bruhwiler, L., Cameron-Smith, P. J., Christensen, J. H.,
554 Delage, F., Denning, A. S., Fan, S.-M., Geels, C., Houweling, S., Imasu, R.,
555 Karstens,U., Kawa, S. R., Kleist, J., Krol, M., Law, R. M., Lin, S.- J., Lokupitiya,
556 R., Maki, T., Maksyutov, S., Niwa, Y., Onishi, R., Parazoo, N., Pieterse, G., Rivier,
557 L., Satoh, M., Serrar, S., Taguchi, S., Takigawa, M., Vautard, R., Vermeulen, A. T.,
558 and Zhu, Z., TransCom model simulations of hourly atmospheric CO_2: Analysis of
559 synoptic-scale variations for the period 2002–2003, Global Biogeochem. Cy., 22,
560 GB4013, doi:10.1029/2007GB003081, 2008.
561 33. Patra, P. K., Houweling, S., Krol, M., Bousquet, P., Belikov, D., Bergmann, D.,
562 Bian, H., Cameron-Smith, P., Chipperfield, M. P., Corbin, K., Fortems-Cheiney, A.,
563 Fraser, A., Gloor, E., Hess, P., Ito, A., Kawa, S. R., Law, R. M., Loh, Z., Maksyutov,
564 S., Meng, L., Palmer, P. I., Prinn, R. G., Rigby, M., Saito, R., and Wilson, C.:
565 Transcom model simulations of CH_4 and related species: linking transport, surface
566 flux and chemical loss with CH_4 variability in the troposphere and lower
567 stratosphere, Atmos. Chem. Phys., 11-12813-12837, doi: 10.5194/acp-11-12813-
568 2011, 2011.
569 34. Rasch, P. J., Boville, B. A., and Brasseur, G. P.: A three dimensional general
570 circulation model with coupled chemistry for the middle atmosphere, J. Geophys.
571 Res., 100, 9041–9071, 1995.
572 35. Raupach, M. R., G. Marland, P. Ciais, C. Le Quere, J. G. Canadell, G. Klepper, and
573 C. B. Field, Global and regional drivers of accelerating CO_2 emissions, Proc. Natl.
574 Acad. Sci. U.S.A., 104(24), 288–293, doi:10.1073/pnas.0700609104, 2007.

575 36. Rayner, P. J., Entiing, I. G., Francey, R. J., and Langenfelds R., Reconstructing the
576 recent carbon cycle from atmospheric CO2, $\delta^{13}C$ and O_2/N_2observations, Tellus,
577 vol. 51B, pp.213-232, 1999.
578 37. Rayner, P. J. and O'Brien, D. M.: The utility of remotely sensedCO_2 concentration
579 data in surface inversion, Geophys. Res. Lett., 28, 175–178, 2001.
580 38. Schoeberl, M. R., Douglass, A. R., Zhu, Z., and Pawson, S.: Acomparison of the
581 lower stratospheric age spectra derived from a general circulation model and two
582 data assimilation systems, J. Geophys. Res., 108, 4113, doi:
583 10.1029/2002JD002652, 2003.
584 39. Scholes, R. J., Monteiro, P. M. S., Sabine, C. L., and Canadell, J. G.: Systematic
585 long-term observations of the global carbon cycle, Trends in Ecology & Evolution,
586 24, 427–430, doi:10.1016/j.tree.2009.03.006, 2009.
587 40. Stohl, A., Cooper, O., and James, P.: A cautionary note on the use of meteorological
588 analysis data for quantifying atmospheric mixing, J. Atmos. Sci., 61, 1446–1453,
589 2004.
590 41. Strow, L. L. and Hannon, S. E.: A 4-year zonal climatology of lower tropospheric
591 CO2 derived from ocean-only Atmospheric Infrared Sounder observations, J.
592 Geophys. Res., 113, D18302, doi: 10.1029/2007JD009713, 2008.
593 42. Tans, P., Fung, I., and Takahashi, T., Observational constraints of the global
594 atmospheric CO2 budget, Science, vol. 247, pp.1431-1438, 1990.
595 43. Thompson, R. L., Ishijima, K., Saikawa, E., Corazza, M., Karstens, U., Patra, P. K.,
596 Bergamaschi, P., Chevallier, F., Dlugokencky, E., Prinn, R. G.., Weiss, R. F.,

597 O'Doherty, S., Fraser, P. J., Steele, L. P., Krummel, P. B., Vermeulen, A., Tohjima,
598 Y., Jordan, A., Haszpra, L., Steinbacher, M., Van der Laan, S., Aalto, T., Meinhardt,
599 F., Popa, M. E., Moncrieff, J., and Bousquet, P., TransCom N_2O model inter-
600 comparison – Part 2: Atmospheric inversion estimates of N_2O emissions, Atmos.
601 Chem. Phys., 14, 6177–6194, doi:10.5194/acp-14-6177-2014, 2014
602 44. Waugh, D. W., and Hall, T. M.: Age of stratospheric air: Theory, observations, and
603 models, Rev. Geophys., 40, 1010, doi: 10.1029/2000RG000101, 2002.
604 45. Weaver, C. J., Douglass, A. R., and Rood, R. B., Thermodynamic balance of three-
605 dimensional stratospheric winds derived from a data assimilation procedure, J.
606 Atmos. Sc., 50, 2987-2993, 1993.
607 46. Wofsy, S. C., Daube, B. C., Jimenez, R., Kort, E., Pittman, J. V., Park, S., Commane,
608 R., Xiang, B., Santoni, G., Jacob, D., Fisher, J., Pickett-Heaps, C., Wang, H., Wecht,
609 K., Wang, Q.-Q., Stephens, B. B., Shertz, S., Watt, A. S., Romashkin, P., Campos,
610 T., Haggerty, J., Cooper, W. A., Rogers, D., Beaton, S., Hendershot, R., Elkins, J.
611 W., Fahey, D. W., Gao, R. S., Moore, F., Montzka, S. A., Schwarz, J. P., Perring, A.
612 E., Hurst, D., Miller, B. R., Sweeney, C., Oltmans, S., Nance, D., Hintsa, E., Dutton,
613 G., Watts, L. A., Spackman, J. R., Rosenlof, K. H., Ray, E. A., Hall, B., Zondlo, M.
614 A., Diao, M., Keeling, R., Bent, J., Atlas, E. L., Lueb, R., Mahoney M. J., 2012.
615 HIPPO Merged 10-second Meteorology, Atmospheric Chemistry, Aerosol Data
616 (R_20121129). Carbon Dioxide Information Analysis Center, Oak Ridge National
617 Laboratory, Oak Ridge, Tennessee, U.S.A.
618 http://dx.doi.org/10.3334/CDIAC/hippo_010, (Release 20121129)

(HIPPO_all_missions_merge_10s_20121129.tbl).

47. Wunch, D., Toon, G., Blavier, J.-F. L., Washenfelder, R.A., Notholt, J., Connor, B.J., Griffith, D.W.T., Sherlock, V., and Wennberg, P.O.: The Total Carbon Column Observing Network (TCCON), Phil. Trans. R. Soc. A369, 2087–2112, doi:10.1098/rsta.2010.0240, 2011.

48. Yang, Z., Washenfelder, R. A., Keppel-Aleks, G., Krakauer, N. Y., Randerson, J. T., Tans, P. P., Sweeney, C., and Wennberg, P. O.: New constraints on Northern Hemisphere growing season net flux P, Geophys. Res. Lett., 34, 1–6, doi: 10.1029/2007GL029742, 2007.

49. Yokota, T., Yoshida, Y., Eguchi, N., Ota, Y., Tanaka, T., Watanabe, H., and Maksyutov, S.: Global concentrations of CO_2 and CH_4retrieved from GOSAT: First preliminary results, SOLA, 5, 160–163, doi:10.2151/sola.2009-041, 2009.

50. Y. Yoshida, N. Kikuchi, I. Morino, O. Uchino, S. Oshchepkov, A. Bril1, T. Saeki, N. Schutgens, G. C. Toon, D. Wunch, C. M. Roehl, P. O. Wennberg, D. W. T. Griffith, N. M. Deutscher, T. Warneke, J. Notholt, J. Robinson, V. Sherlock, B. Connor, M. Rettinger, R. Sussmann, P. Ahonen, P. Heikkinen, E. Kyrö, J. Mendonca, K. Strong, F. Hase, S. Dohe, and T. Yokota, Improvement of the retrieval algorithm for GOSAT SWIR XCO_2 and XCH_4 and their validation using TCCON data, Atmos. Meas. Tech., 6, 1533-1547, doi:10.5194/amt-6-1533-2013, 2013.

641

642

643

644

645

646

647

648

649

650

651

652

653

654

655

656 *Table 1.Vertical grid levels of the NIES TM model

	H, km	σ=P/P_s	≈△, m	ξ(σ-θ grid levels), K	Number of levels
Near-surface layer	0-2	1.0−0.795	250	−	8
Free troposphere	2-12	0.795−0.195	1000	−, 330,350,	10
Upper troposphere and stratosphere	12−40	0.195-0.003	1000 2000 −	365,380,400,415, 435,455,475,500, 545, 590,665,850, 1325,1710	14
				Total levels:	32

657

*H, height; P, atmospheric pressure; P_s, surface atmospheric pressure; △, vertical integral step; ξ, the level of the sigma-isentropic grid.

658 Table 2.Temporal and spatial (horizontal) coverage of HIPPO mission flights.

Missions	Sampling Dates	Vertical Profiles Flown	Flight Path Notes
HIPPO-1	January 8–30, 2009	138	Northern polar flight #1 reached 80 ºN, Southern ocean flight reached 67 ºS, 175 ºW (no return to the Arctic a second time).
HIPPO-2	October 31 to November 22, 2009	148	Northern polar flight #1 reached 80 ºN, Southern ocean flight reached 66 ºS, and 174 ºW, Northern polar flight #2 reached 83 ºN.
HIPPO-3	March 24 to April 16, 2010	136	Northern polar flight #1 reached 84.75 ºN, Southern ocean flight reached 66.8 ºS, 170 ºE, Northern polar flight #2 reached 85 ºN.

659

660

661

662

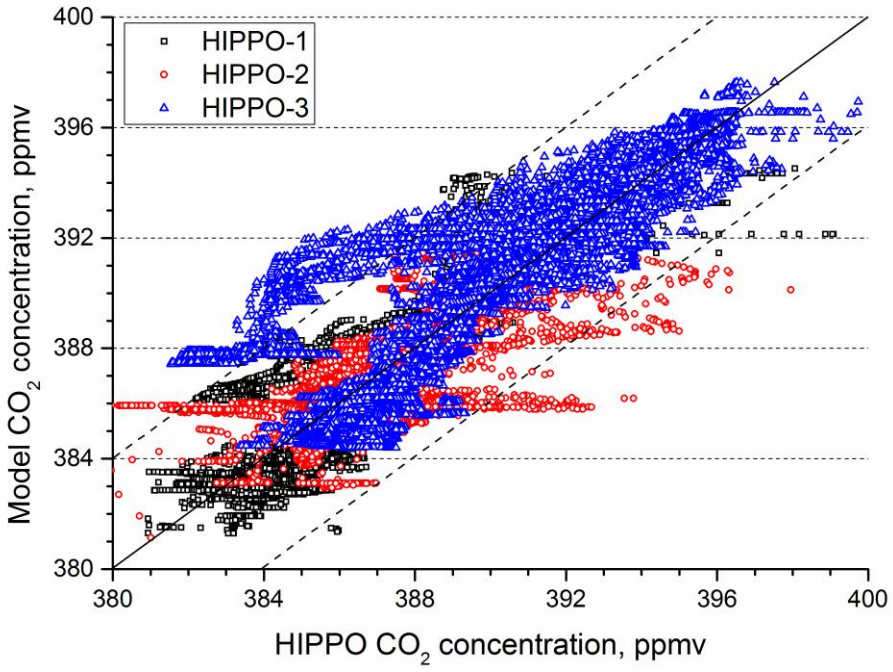

663

664 **Figure 1.** Scatter diagram of modeled and observed CO_2 of HIPPO-1 (black square), 2

665 (red circle), 3 (blue triangle). Dotted lines show a 95% confidence interval

of CO_2 concentration.

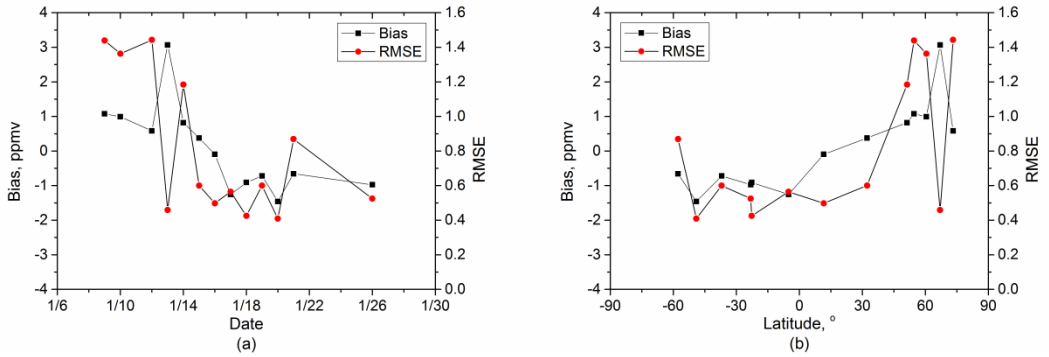

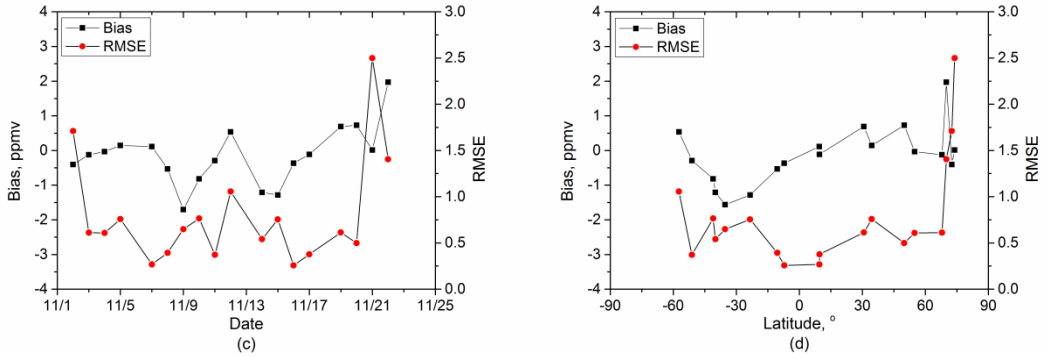

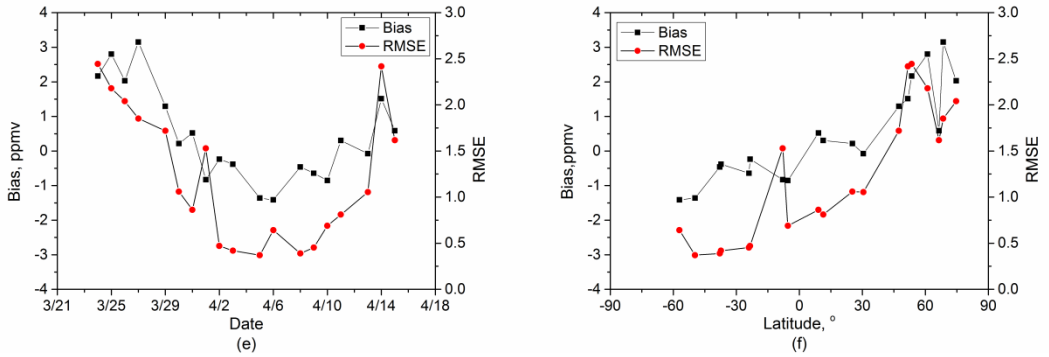

Figure 2. Bias (simulation-observation, black square) and RMSE (red circle) of time- ((a) HIPPO-1, (c) HIPPO-2, (e) HIPPO-3) and latitude-varying ((b) HIPPO-1, (d) HIPPO-2, (f) HIPPO-3) CO_2 concentration data.

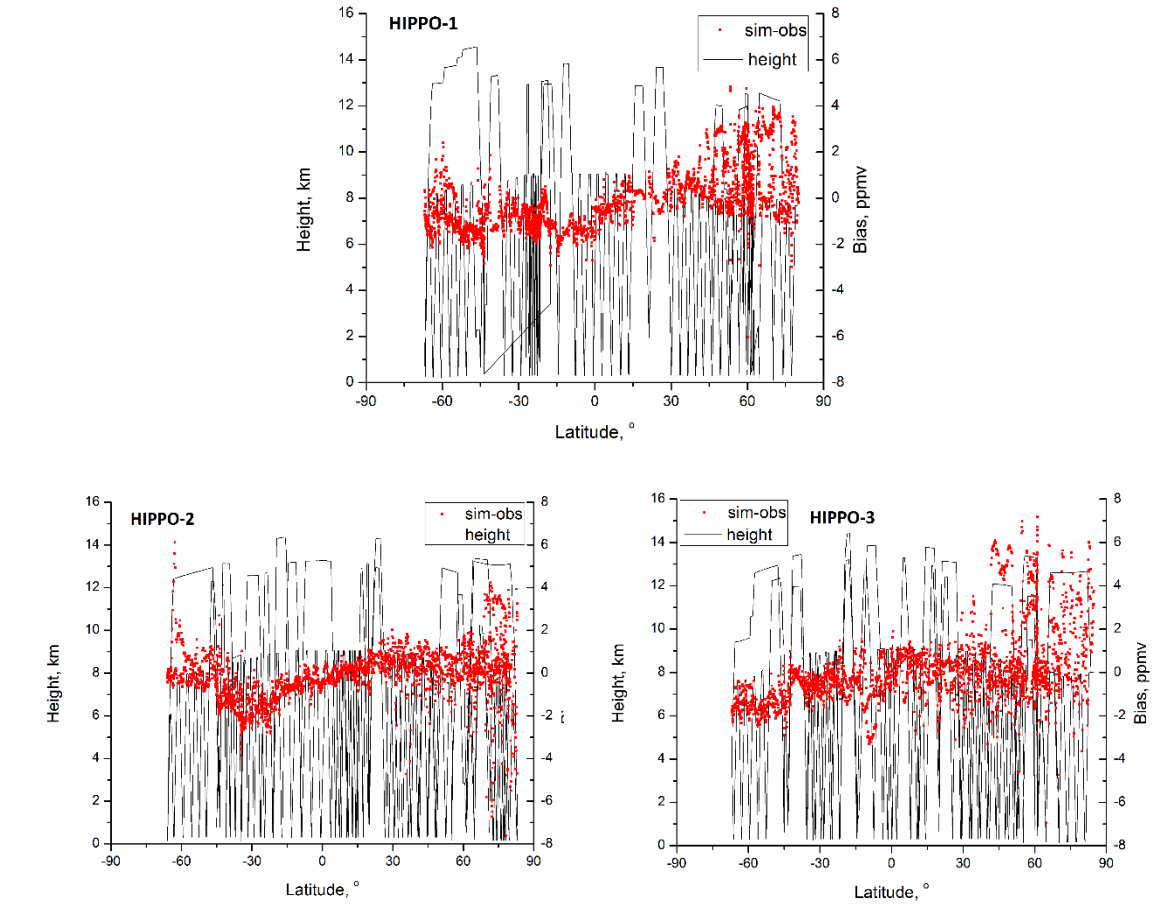

Figure 3. Change of flight height and difference between simulation and observation of HIPPO-1, 2, 3 with latitude.

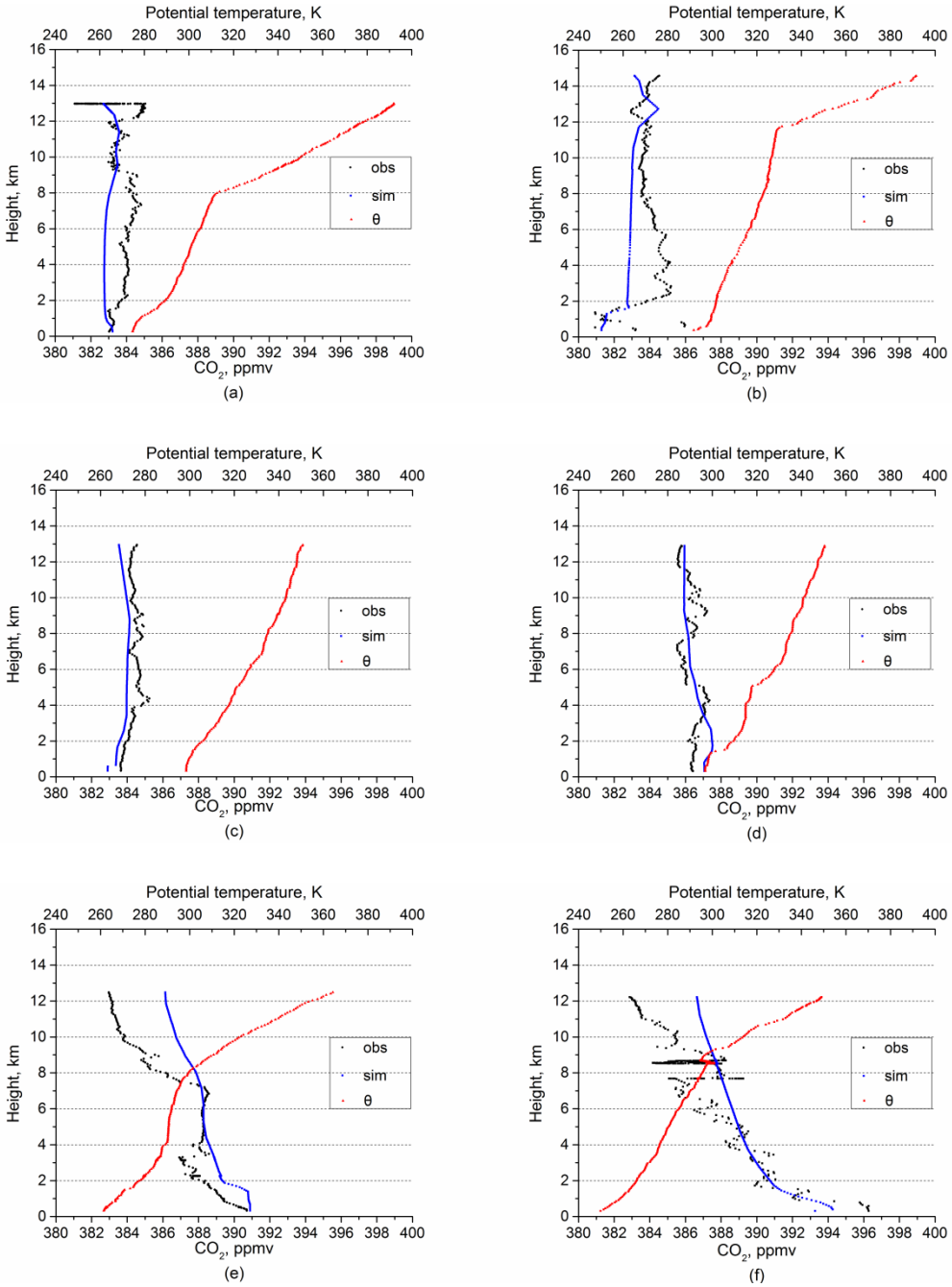

Figure 4. Vertical profiles from near-surface to the LS for HIPPO-1, panels represent the vertical profiles of observation (black square), simulation (blue square) and potential temperature (red square) in Southern ((a) high-, (b) mid-, (c)

low- latitude), and Northern Hemisphere ((d) low- , (e) mid-, (f) high-latitude).

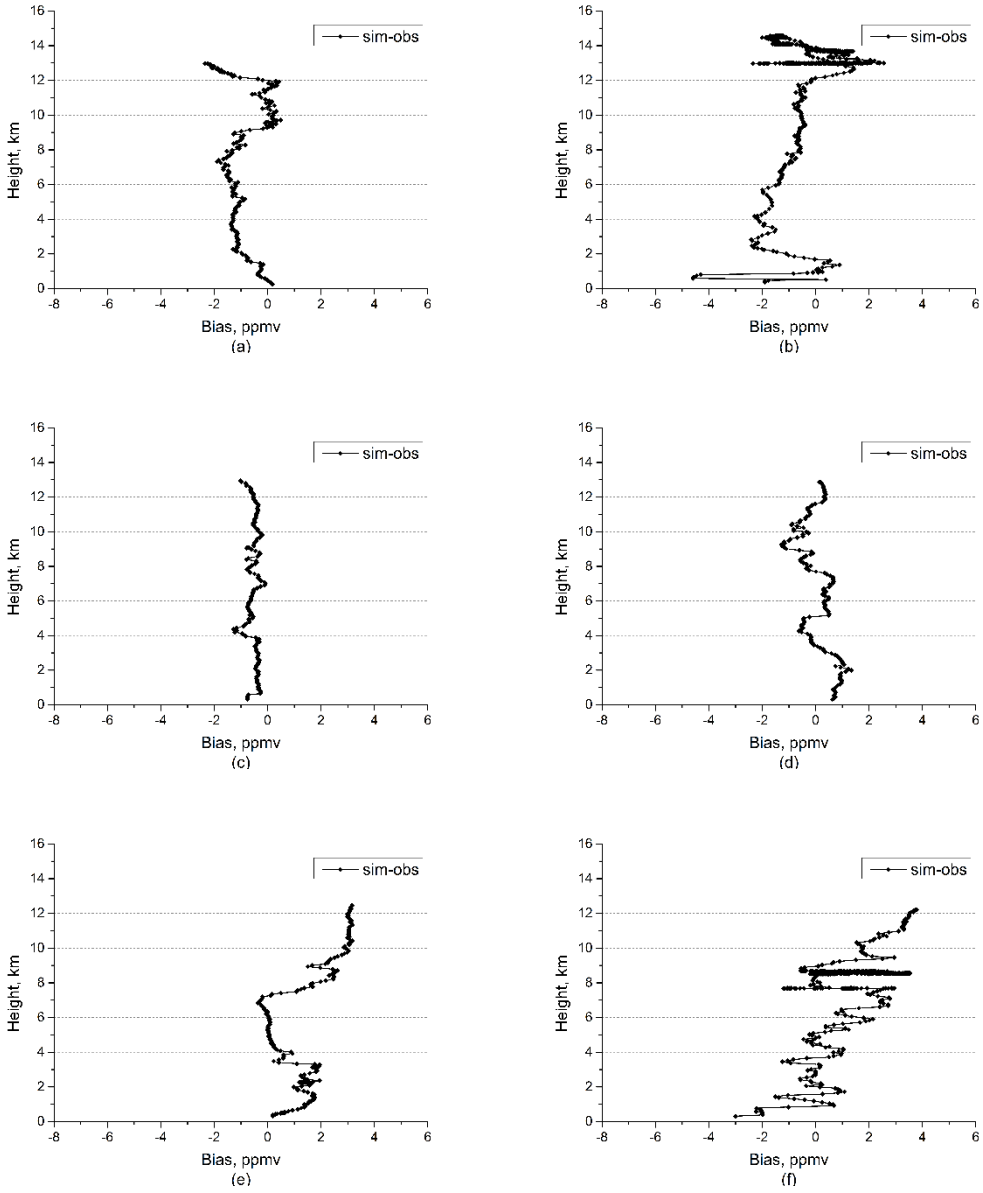

Figure 5. Biases of simulation minus observation from near-surface to the LS for HIPPO-1, panels are corresponding to Figure 4(a)-4(f) respectively.

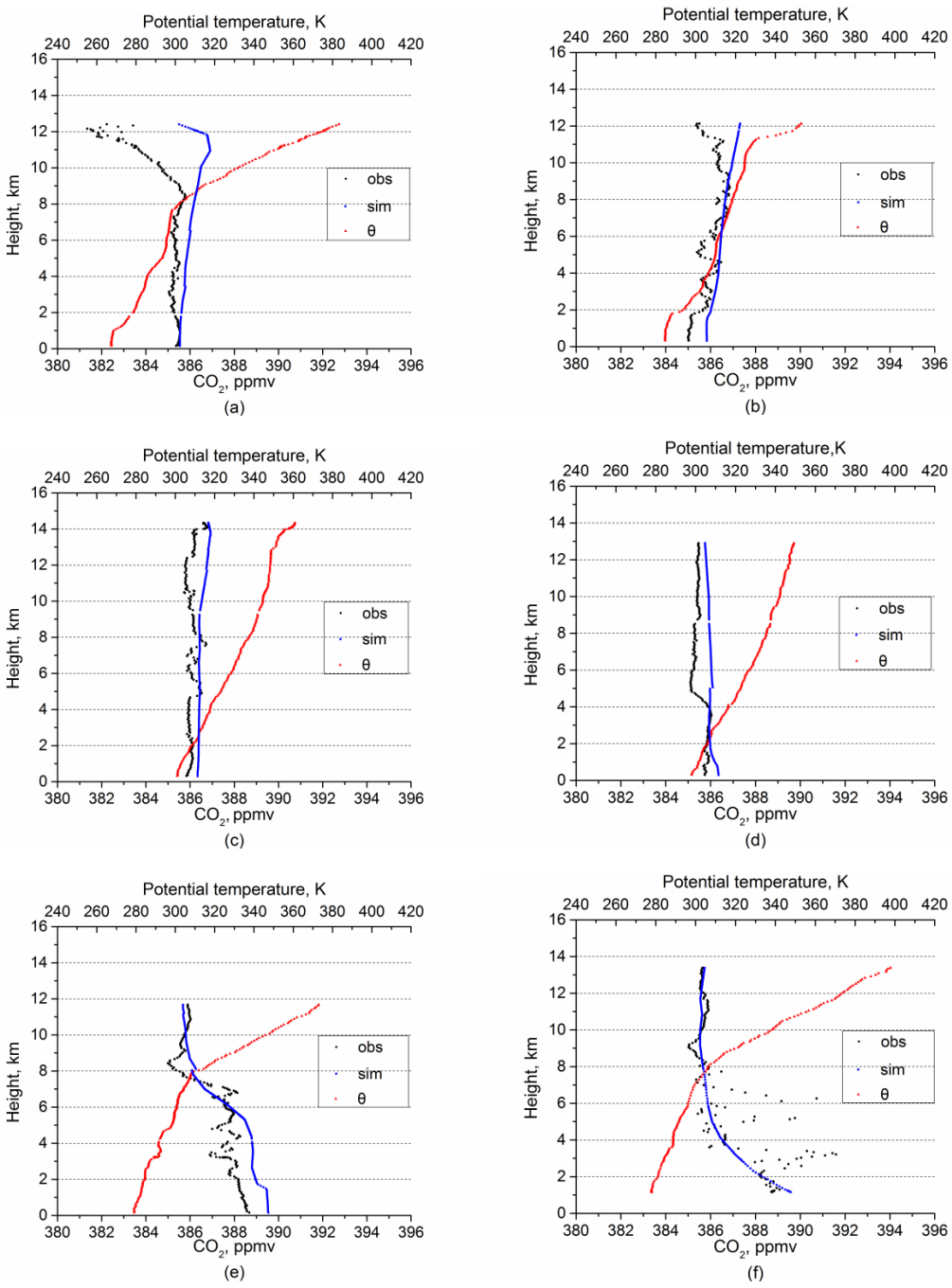

Figure 6. The vertical profiles from near-surface to the LS for HIPPO-2, panels represent the vertical profiles of observation (black square), simulation (blue square) and potential temperature (red square) in Southern ((a) high-, (b) mid-, (c) low- latitude), and Northern Hemisphere ((d) low-, (e) mid-, (f) high- latitude).

738

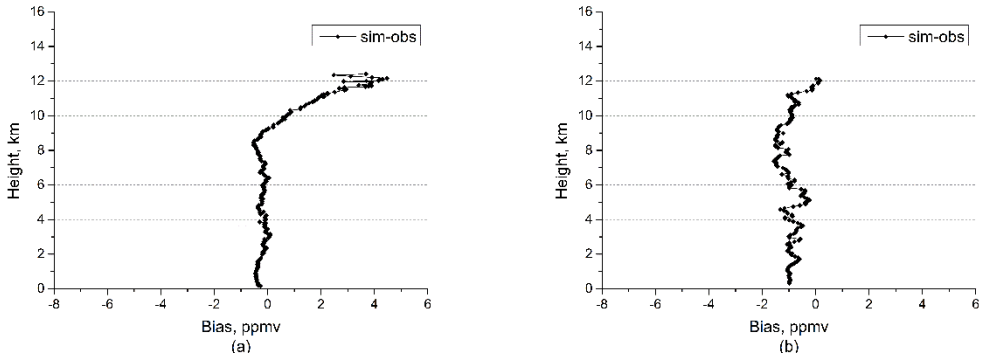

739

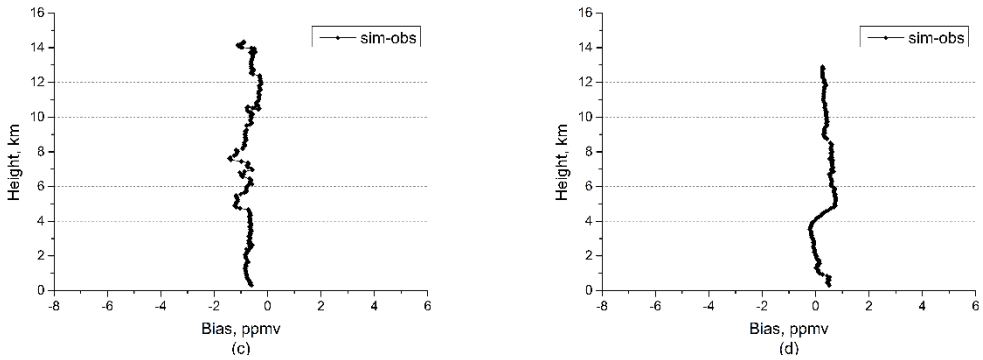

740

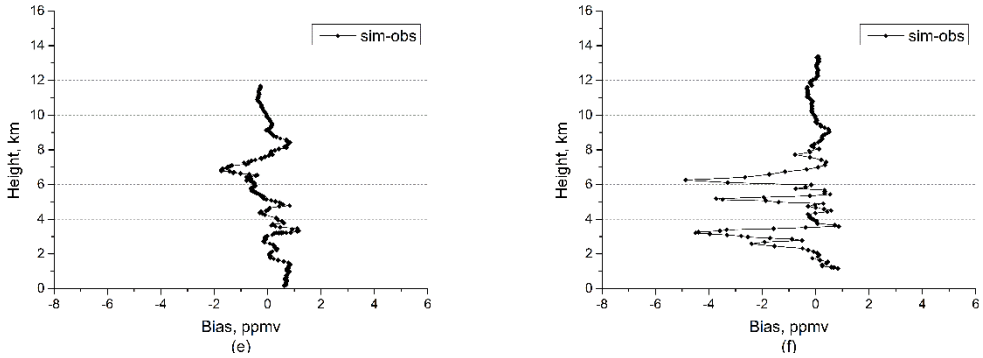

741 **Figure 7.** Biases of simulation minus observation from near-surface to the LS for
742 HIPPO-2, panels are corresponding to Figure 6(a)-6(f) respectively.

743

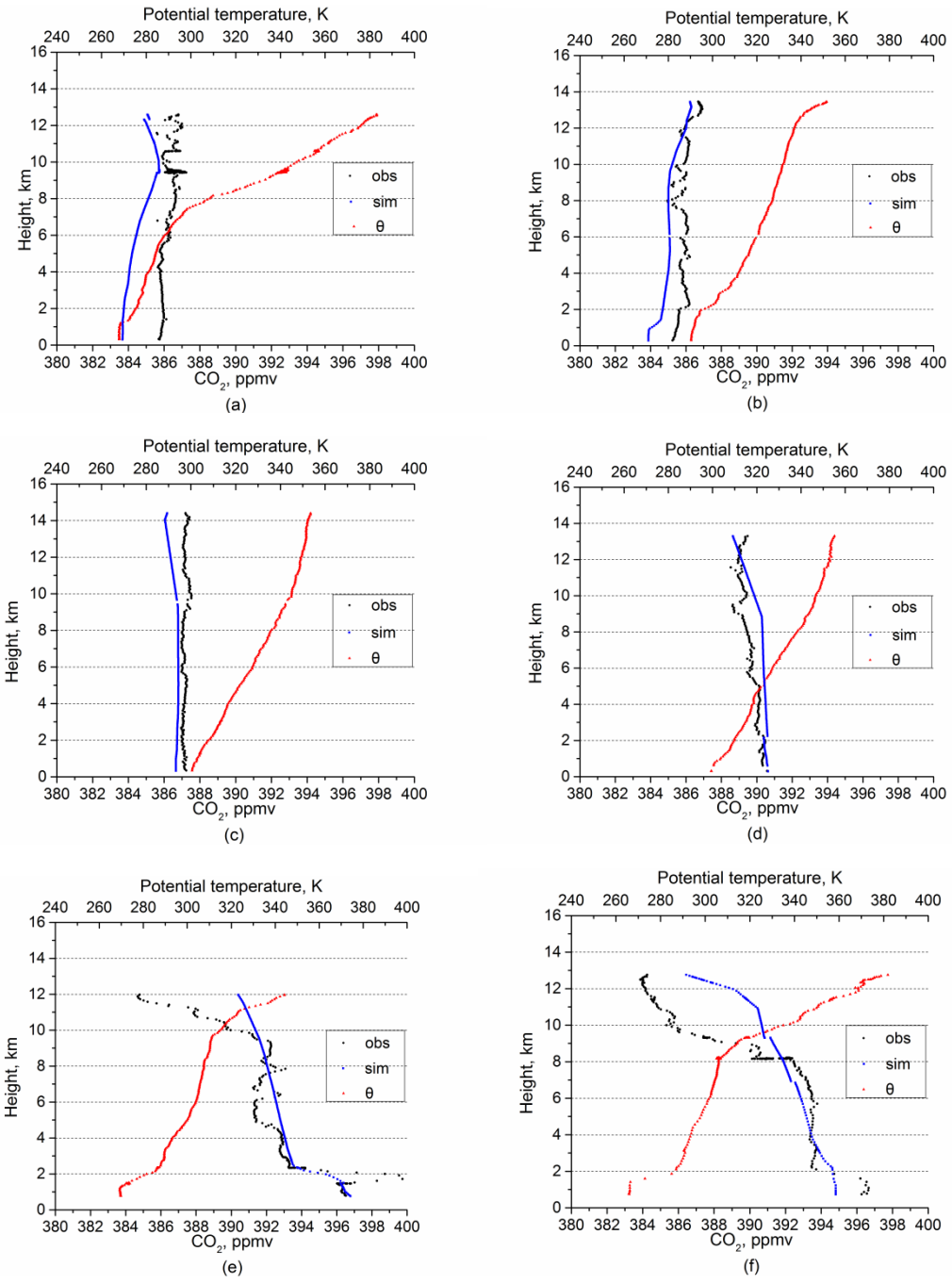

Figure 8.The vertical profiles from near-surface to the LS for HIPPO-3, panels represent the vertical profiles of observation (black square), simulation (blue square) and potential temperature (red square) in Southern ((a) high-, (b) mid-, (c) low- latitude), and Northern Hemisphere ((d) low-, (e) mid-, (f) high- latitude).

753

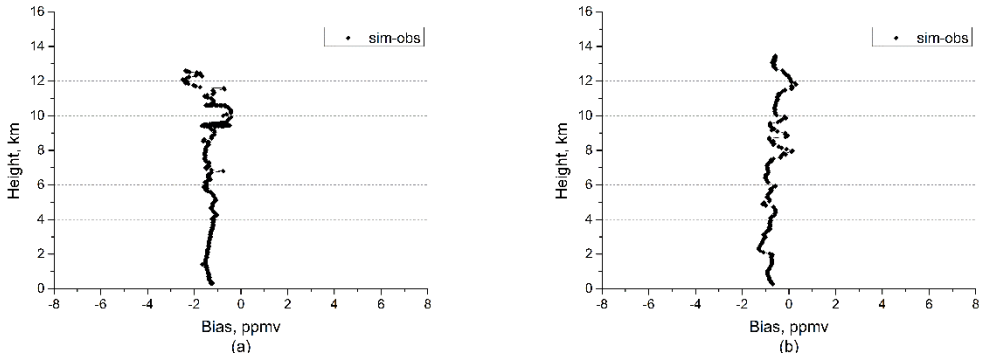

754

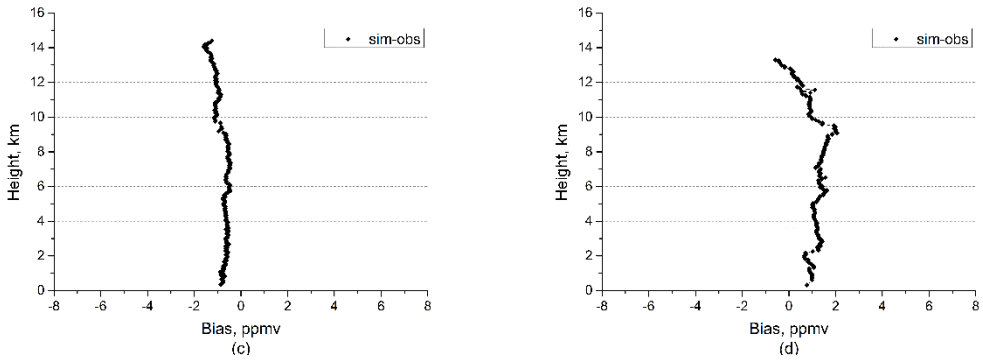

755

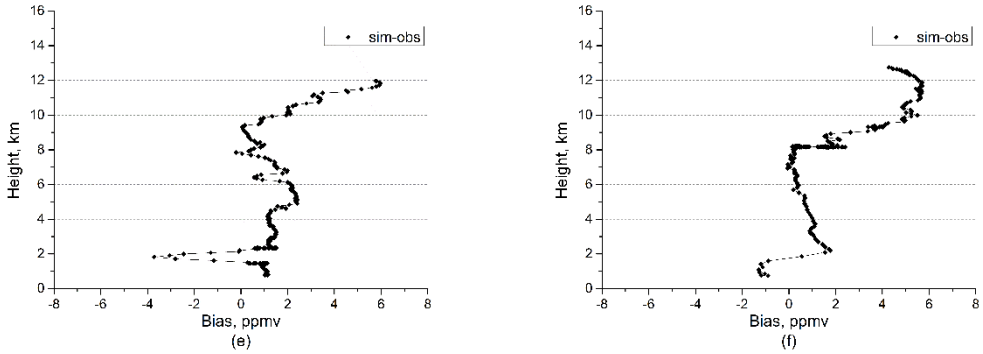

756 **Figure 9.** Biases of simulation minus observation from near-surface to the LS for
757 HIPPO-3, panels are corresponding to Figure 8(a)-8(f) respectively.

758